Volume 13
Number 14
21 July 2025
Pages 3725-3994

Biomaterials Science

rsc.li/biomaterials-science

ISSN 2047-4849

ROYAL SOCIETY OF CHEMISTRY

PAPER
Raechelle A. D'Sa *et al.*
Antimicrobial 3D printed gelatin scaffolds for root canal disinfection in regenerative endodontics procedures

European Society for Biomaterials

Biomaterials Science

ROYAL SOCIETY OF CHEMISTRY

PAPER

View Article Online
View Journal | View Issue

Cite this: *Biomater. Sci.*, 2025, **13**, 3795

Antimicrobial 3D printed gelatin scaffolds for root canal disinfection in regenerative endodontics procedures

Mateo Dallos Ortega,[a] Jenny Aveyard,[a] Raghda Magdy Abdelgawad,[b,e] Reem El-Gendy,[b,d] Alexander Ciupa,[c] David Whetnall,[c] Julia Behnsen,[a] Robert J. Poole[a] and Raechelle A. D'Sa*[a]

Received 19th March 2025,
Accepted 1st May 2025

DOI: 10.1039/d5bm00440c

rsc.li/biomaterials-science

Regenerative endodontic procedures (REPs) which aim to promote root development and pulp tissue regeneration in necrotic immature teeth, have emerged as a promising therapeutic approach. A critical determinant of REP success hinges on effective disinfection of the root canal system, which must eliminate microbial contaminants whilst preserving the microenvironment necessary for dental pulp stem cell tissue regeneration. This study reports on the fabrication of biocompatible 3D printed hydrogel scaffolds designed for root canal disinfection. The scaffolds incorporate benzyldimethyldodecylammonium chloride (BDMDAC) a broad-spectrum quaternary ammonium compound characterised by low cytotoxicity and minimal risk of resistance development. BDMDAC loaded gelatin biomaterial inks were systematically evaluated for rheology properties, mechanical stability and drug release properties. Scaffolds containing 150 μg mL^{-1} and 250 μg mL^{-1} BDMDAC exhibited excellent antimicrobial efficacy against 5 bacterial pathogens (including 3 endodontic bacteria-*Enterococcus faecalis*, *Porphyromonas gingivalis*, and *Streptococcus mutans*). Cytocompatibility assays using primary human dental pulp stem cells (HDPSCs) derived from 3 donors confirmed over 70% of cell viability. Furthermore, freeze-dried scaffolds demonstrated excellent shelf-life stability for at least six months. Overall, these findings highlight the potential of 3D printed BDMDAC-loaded 3D printed gelatin scaffolds as an effective and cytocompatible platform for root canal disinfection in REPs.

1. Introduction

Regenerative endodontic procedures (REPs) which aim to promote root development and pulp tissue regeneration, have emerged as a promising treatment modality for necrotic immature teeth. Traumatic injuries or dental disease cause inflammation, pulp necrosis and loss of immature permanent teeth.[1] Pulp necrosis is a significant issue affecting children and adolescents worldwide.[1] In order to enable full root growth in permanent immature teeth, modern regenerative endodontic procedures (REPs) can be used to restore the health and function of damaged or diseased dental pulp.[1,2] Endodontic procedures, as outlined by the American Association of Endodontists (AAE) and the European Society of Endodontology (ESE), follow a systematic, evidence-based approach beginning with diagnosis through clinical and radiographic evaluation, and the use of local anaesthesia for patient comfort. In REPs, treatment starts with irrigation—typically using sodium hypochlorite—followed by placement of an intracanal medicament such as triple antibiotic paste.[3,4] This medicament is applied after irrigation and often remains in the canal for more than seven days, depending on clinical needs. Once disinfection is achieved, bleeding is induced from periapical tissues to form a blood clot that serves as a scaffold for progenitor cell recruitment and pulp-like tissue regeneration.[1,2]

Over the past decade, significant advancements have been made in biocompatible root canal disinfection including the characterisation of human dental pulp stem cells (HDPSCs)[5,6] and the development of antimicrobial hydrogel scaffolds.[7–11] Whilst these scaffolds have enhanced REP procedures, challenges remain in eliminating resistant microorganisms and residual bacteria during disinfection which could disrupt the HDPSC microenvironment, compromising treatment outcomes.[12–14]

[a]*School of Engineering, University of Liverpool, Harrison Hughes Building, Brownlow Hill, Liverpool, L69 3GH, UK. E-mail: r.dsa@liverpool.ac.uk*
[b]*Division of Oral Biology, School of Dentistry, University of Leeds, Leeds LS9 7TF, UK*
[c]*Materials Innovation Factory, University of Liverpool, 51 Oxford Street, Liverpool L7 3NY, UK*
[d]*Department of Oral Pathology, Faculty of Dentistry, Suez Canal University, Egypt*
[e]*Department of Endodontics, Faculty of Dentistry, Assiut University, Assiut 83523, Egypt*

The persistence of pathogens or residual biofilms in the root canal space of immature permanent teeth remains a major obstacle to the success of REPs.[15,16] A recent systematic review by Almutairi *et al.* reported that 79% of failed clinical cases were attributed to persistent infections,[17] underscoring infection control as the critical determinant of REP success.[18] Histological analyses reveals that current disinfection methods often require antibiotic concentrations that can be cytotoxic and may affect the bioavailability of growth factors resulting in impaired tissue regeneration.[19–21] In response to the limitations of limited efficiency, rising levels of drug resistance and potential toxicity, recent efforts have focused on developing alternative antimicrobials agents.[7,22,23]

Quaternary ammonium compounds (QACs) are potent broad-spectrum biocides with low toxicity and are widely employed the pharmaceutical and medical applications.[24] As surfactants, QACs possess a hydrophilic head and a hydrophobic tail, the length of which influences their antimicrobial efficacy.[25] QACs exhibit broad-spectrum activity and have demonstrated excellent efficacy for the treatment of dental carries and periodontitis.[25,26] Imazato *et al.* demonstrated that 5% methacryloyloxydodecylpyridinium bromide (MDPB), a QAC, significantly inhibits cariogenic microbes such as *Actinomycetes* and *Candida albicans*.[27] MDPB is also effective against anaerobic bacteria, including clinical isolates of *Streptococcus mutans*, *Streptococcus sobrinus* SL-1, *Streptococcus oralis*, and *Streptococcus sanguinis*, which are in dental pulp infections.[28] Moreover, MDPB outperforms chlorohexidine (CHX) in disinfection and preventing apical periodontitis.[29] Kumar Tiwari *et al.* further reported that QACs such as dimethylaminododecyl methacrylate (DAMDDM) and dimethylaminohexadecyl methacrylate (DMAHDM) are more effective than CHX in eradicating endodontic bacteria and their biofilms.[30]

Disinfection of the root canal with QACs and other antiseptics is typically achieved using irrigants or antibiotic pastes. However, these methods often suffer from limited penetration into infected tissues and insufficient duration of action to prevent secondary infections. Additionally, the concentration required for antimicrobial efficacy can negatively impact HDPCs survival and function, compromising tissue regeneration. To address these limitations, biocompatible drug delivery systems have been explored to enable controlled and sustained release of antimicrobials, enhancing disinfection efficacy.[12–14]

Gelatin based hydrogels have gained prominence in this context due to their inherent biocompatibility, ease of modification, degradability, and rapid gelation induced by low temperature.[25] Ribeiro *et al.* developed photocrosslinkable chlorhexidine-loaded methacrylated gelatin (GelMA) hydrogels with broad spectrum of antimicrobial activity with total inhibition of biofilms of endodontic pathogens *Enterococcus faecalis* and *Actinomyces naeslundii*.[31] In a subsequent study, Ribeiro *et al.* have fabricated GelMA hydrogels containing clindamycin- or metronidazole-laden electrospun poly DL-lactide-*co*-glycolide (PLGA) fibers. The clindamycin-containing hydrogel systems demonstrated antimicrobial efficacy against all bacterial species tested (*Actinomyces naeslundii*, *Fusobacterium nucleatum*, and *Enterococcus faecalis*) and promoted the formation of capillary-like networks of endothelial cells *in vitro* alongside widespread vascularization and functional blood vessels formation *in vivo*.[32]

Primary root canal infections are dominated by Gram-negative bacteria with at least 10–30 species present per canal.[33] Following treatment, the microbial diversity decreases significantly with 1–5 predominantly Gram-positive anaerobes remaining.[34,35] with *Enterococcus faecalis* being the species most frequently associated with cases of endodontic failure.[36–38] Although, *E. faecalis* normally resides in the gastrointestinal tract, it can colonize the root canals and dentinal tubules of infected teeth. It can withstand harsh conditions such as starvation and alkaline pH, and form resilient biofilms.[39–41] These survival strategies likely contribute to its persistence despite conventional disinfection methods.[38,42] Consequently any antimicrobial strategy for root canal disinfection must be evaluated for its efficacy against *E. faecalis*.

This study presents the development of 3D-printed hydrogel scaffolds incorporating varying concentrations of a QACs to create a biocompatible and antibacterial platform suitable for REPs. Benzyldimethyldodecylammonium chloride (BDMDAC), a C12-alkyl QAC previously used in dental adhesives and denture base resins was selected as the model antimicrobial.[43] BDMDAC was loaded in to gelatin-based formulations at varying concentration to produce 3D printable biomaterial inks optimised for rheological performance, enabling ease of printability, shape fidelity post printing and mechanical stability. The release kinetics and concentration profiles for BDMDAC from the scaffolds were quantified using high performance liquid chromatography (HPLC). To enhance shelf-life, the printed scaffolds were freeze-dried. The antimicrobial and antibiofilm efficacy of the scaffolds were studied against Gram positive methicillin resistant *Staphylococcus aureus* (MRSA), Gram negative *Pseudomonas aeruginosa* and three prevalent endodontic pathogens*: Enterococcus faecalis*, *Porphyromonas gingivalis*, and *Streptococcus mutans.* Cytocompatibility of the most optimised scaffolds were evaluated using primary HDPSCs derived from three donor patients.

2. Materials and methods

2.1 Materials

150 bloom gelatin A from bovine skin, benzyl dimethyl dodecyl ammonium chloride (BDMDAC), Glutaraldehyde 50 wt% in H_2O solution, ethanol, nutrient agar (NA), nutrient broth (NB), Luria Broth (LB), Luria Agar (LA), tryptic soy broth (TSB), tryptic soy agar (TSA), menadione (vitamin K3), hemin from porcine (Sigma-Aldrich), Columbia broth (CB), Columbia agar (CA) and defibrinated sheep blood (Darwin Biological).

2.2 Gelatin-BDMDAC bioink preparation

A 5% w/w gelatin bioink (GL5) was prepared as follows: 0.25 g of gelatin was added to 5 g of distilled water at 60 °C and

Table 1 Nomenclature of gel (GL-) and freeze dried (FGL-) gelatin-BDMDAC ink composition

Sample name		BDMDAC concentration (μg mL^{-1})
Freeze dried	**Gel**	—
FGL5-Q3.9	GL5-Q3.9	3.9
FGL5-Q7.8	GL5-Q7.8	7.81
FGL5-Q15	GL5-Q15	15.6
FGL5-Q31	GL5-Q31	31.2
FGL5-Q62	GL5-Q62	62.5
FGL5-Q125	GL5-Q125	125
FGL5-Q250	GL5-Q250	250
FGL5-Q500	GL5-Q500	500
FGL5-Q1000	GL5-Q1000	1000

stirred at 600 RPM until a homogenous solution was acquired (1 h). For the BBDAC-loaded gelatin inks (GL5-Q) varying concentrations of BBDAC (0.39, 0.781, 0.156, 0.312, 0.625, 0.125, 0.25, 0.5, 1 mg mL^{-1}) were added to water preheated at 60 °C and stirred at 600 RPM for one hour. The inks were loaded into 3 mL cartridges at room temperature 30 minutes before printing. FGL5-Q denotes freeze dried scaffolds with varying BDMDAC concentrations. The synthesis of the various inks has been shown previously.[7] The nomenclature and conditions for all sample types are listed in Table 1.

2.3 3D printing

The structure of the 3D printed scaffolds was designed using 3D CAD drawing software (Creo Parametric®) to generate stereolithography (STL) files and converted to a G-code generator (Slic3r) which is integrated in Cellink's operating software (DNA®). During the slicing process, the layer height, printing speed and infill percentage were defined. The infill percentage is one of the most important features for 3D printing as it determines the pore size by defining the distance between two adjacent filaments. The 3D structures were printed by dual printhead extrusion-based 3D printer (BIOX6, Cellink®) using a 27G nozzle at 28 °C with a pressure range between 100–115 kPa and a printing speed of 10 mm s^{-1}. The final construct was made of twelve 0.2 mm layers, with an infill percentage of 20% giving a 2.5 mm distance between each adjacent filament. The scaffold dimensions were 10 × 10 × 2.5 mm. After printing, the scaffolds were crosslinked with a 0.5% glutaraldehyde solution for 30 minutes on a shaker plate at 50 rpm. Unreacted glutaraldehyde was removed by washing scaffolds three times with water for five minutes each. Finally, scaffolds were sterilized with UV light (265 nm) for 30 minutes before use. In order to enhance the durability and longevity of the scaffolds, freeze-drying was employed. Freeze-drying, also known as lyophilization, is a process wherein the scaffolds are subjected to low temperatures and reduced atmospheric pressure to remove moisture content. This dehydration method not only aids in preventing degradation but also contributes significantly to extending the shelf life of the scaffolds, ensuring their structural integrity and functional efficacy over an extended period.[44] The scaffolds were frozen at −18 °C and lyophilized for 24 h in a freeze dryer (Scanvac CoolSafe Touch 110-4, Denmark).

2.4 Rheological analysis

The rheological properties of the inks were measured using oscillatory shear experiments in an HTR 502 modular compact rheometer (Anton Paar, Ostfildern, Germany) equipped with a 40 mm diameter parallel rough plate (top and surface) to minimise slip, and a solvent trap to prevent hydrogel evaporation. Rheological assays were performed by injecting the hydrogel directly onto the platform. The rough plate was lowered to a gap height of 1 mm. Once the upper plate was lowered, the platform was heated to 40 °C to heal any fractures in the gel. Excess hydrogel was trimmed, and the sample was allowed to cool to room temperature (21 °C).

Rheological measurements for all samples were conducted in triplicate, and the results are presented as the average of the three tests. A temperature sweep was performed at 0.5% strain amplitude and a frequency of 1 Hz, cooling the samples from 40 °C to 15 °C at a rate of 1 °C min^{-1}. Strain amplitude sweep tests were conducted to determine the linear viscoelastic region, within a strain range of 0.1–1000%, at a constant frequency of 1 Hz. Following this, frequency sweep tests were performed at 0.5% strain, with a frequency range from 0.1 to 10 Hz. The complex viscosity (η^*) was calculated using the storage modulus (G') and loss modulus (G'') obtained from the frequency sweep test. All measurements were conducted at room temperature (21 °C) with a Peltier plate to whiting ±0.1 °C.

2.5 Filament collapse test, diffusion rate and printability

The filament collapse test was conducted as reported previously.[7,45,46] An extruded filament is printed over a stage to evaluate its collapse by measuring its mid-span deflection. The stage was designed using Creo Parametric ®. The stage consisted of seven pillars with incremental distances of 1 mm, ranging from 1 mm to 6 mm. The middle pillars measured 2 × 10 × 6 mm, while the two corner pillars measured 5 × 10 × 6 mm. The design was printed using an Up Mini 2 3D printer with polylactic acid (PLA) filament. The ink was deposited as a single filament on top of the platform. A Sony IMX 682 64 MP 1/1.73″ camera was used to immediately capture an image of the deposited filament to identify the initial conditions of the beam. The pressure, temperature, extrusion velocity, and nozzle diameter were consistent with the parameters used for printing the scaffolds. To determine the collapse area factor (C_f) the following equation was used:[45,47,48]

$$C_f\,(\%) = 100 - \left(\frac{\text{real area}\,(A_a)}{\text{theoretical area}\,(A_t)} \times 100\right) \quad (1)$$

If the ink is unable to bridge between two pillars due to its density, the real area would be considered zero, resulting in a collapse area factor of 100%. If the ink successfully bridges between two pillars, the actual and theoretical areas will be identical, and the collapse area factor will be zero.

For the diffusion rate test, scaffolds with two consecutive layers were printed in a 0–90° pattern, with distances between adjacent filaments increasing from 1 mm to 5 mm in 1 mm increments. To prevent time-dependent deformation measure-

ments, images of the printed scaffolds were taken immediately after fabrication using a Sony IMX 682 64 MP 1/1.73″ camera. The printing speed, temperature, pressure, and nozzle diameter were consistent with previous settings. To calculate the diffusion rate (D_{fr}) and printability (P_r), the following equations were used:[45,47,48]

$$D_{fr} = \frac{PA_t - PA_r}{PA_t} \times 100 \quad (2)$$

$$Pr = \frac{L^2}{16PA_r} \quad (3)$$

where PA_t and PA_r are theoretical and real area of a pore, respectively. L is the real perimeter of the pore. The diffusion rate of the ink without any spreading is 0, while the printability would be 1 for a perfect square.

2.6 Morphological features (μ-CT) and porosity

The morphological features of the scaffold were analysed by micro X-ray computed tomography (μ-CT). The gel, freeze-dried, and re-hydrated samples were scanned with a Zeiss Xradia Versa 620 X-ray microscope. Two scans were carried out of each sample, one encompassing the full sample with a voxel size of 16.8 μm (0.4× objective), and one showing just a corner of the sample in higher resolution (4 μm voxel size, 4× objective). Both scans were acquired using a source accelerating voltage of 60 kV at 6.5 W, without a beam filter, exposure times of 1s per images, and 1601 projection images for the full scan over 360 degrees. The projection data was reconstructed with Zeiss proprietary software Scout-and-Scan Reconstructor version 16.8, using the DeepRecon image improvement option to reduce image noise and enhance image quality.

All measurements were carried out in the open source, image analysis software "Fiji".[49] For volume, surface area, and total porosity quantifications, the 16.8 μm data sets of the whole gel, freeze-dried, and rehydrated samples were binarized and measured using the BoneJ plugin.[50] To measure individual pores and determine the pore size distribution, individual pores in the 4 μm data sets of freeze-dried and re-hydrated gels were segmented using a 3D distance-map based watershed algorithm from the MorphoLibJ plugin.[51] Pores open to the surface, including the large grid structure pores from printing, were excluded from quantification, which was carried out with BoneJ's Particle Analyser plugin.[50] Visualisation images of the sample and the segmented pores were created using Drishti 3.2.[52]

2.7 Swelling ratio of the hydrogel

The swelling performance of the scaffolds was evaluated by immersing the samples in sterile PBS at 37 °C for 72 hours, with measurements taken every 6 hours. The swelling rate (Sw%) was calculated using the following formula[53,54] :

$$Sw\% = \frac{W_w - W_d}{W_d} \times 100 \quad (4)$$

where W_w and W_d denote weight at the swollen and dry state. Excess water was first absorbed with laboratory paper towels. Measurements were done in triplicate.

2.8 Degradation

To calculate the degradation rate, the samples were immersed in PBS and incubated at 37 °C. Every 6 hours, up to a total of 72 hours, the scaffolds were removed, and weighed. Any excess liquid was removed with paper towels. The remaining weight of the scaffold after degradation was determined using the following equation:[53,54]

$$\text{Weight remaining}\,(\%) = 100 - \left[\frac{W_0 - W_f}{W_0} \times 100\right] \quad (5)$$

where W_0 is the initial weight of the scaffold and W_f is the final weight of the scaffold.

2.9 BDMDAC release

The BDMDAC release from the scaffold was determined by high-performance liquid chromatography (HPLC) using the Agilent Technologies 1260 Infinity II System (Radnor, USA) under isocratic conditions at room temperature and equipped with a 4.6 × 250 mm ZORBAX SB-C18 analytical column. Multiple scaffolds were printed and submerged in 1 mL of DI water at 37 °C for different time durations. Then, each aliquot was centrifuged at 4000*g* for 15 minutes, and any undissolved gelatin-BDMDAC was filtered through the protein concentrator. A mixture of acetonitrile (80% in 0.1% formic acid) and water (20%) was used as the mobile phase, at a flow rate of 1 mL min^{-1}, with UV detection at 254 nm and an 8 nm bandwidth. For the HPLC samples, an injection volume of 50 μL, handled by a (G7129A) autosampler, was used. The quantification of the concentrations was determined by the peak area.

2.10 Antimicrobial assay (planktonic)

Overnight cultures of methicillin-resistant *Staphylococcus aureus* (*MRSA*) NCTC 13142 *Pseudomonas aeruginosa* (*P. aeruginosa*) NCTC 07244, *Porphyromonas gingivalis* (*P. gingivalis*) NCTC 11834 and *Enterococcus faecalis* (*E. faecalis*) NCTC 13779 and *Streptococcus mutans* (*S. mutans*) NCTC 10449 were prepared by statically incubating MRSA in nutrient broth, *P. aeruginosa*, in Luria–Bertani broth (LB) at 37 °C for 24 hours. *E. faecalis and P. gingivalis* were incubated in tryptic soy broth (TSB) enriched with hemin (5 mcg mL^{-1}) and menadione (1 mcg mL^{-1}) for 24 and 60 hours, respectively. *S. mutans* was incubated in Columbia broth (CB) at 37 °C for 24 hours. The resulting cultures were diluted to a cell concentration of 10^6 colony forming units per millilitre (CFU mL^{-1}) using a 0.5 McFarland standard.[55] 3D printed scaffolds were inoculated with 1 mL of the diluted cultures and incubated in a shaking incubator at 37.0 °C for 4 and 24 hours. For *P. gingivalis*, samples were incubated in anaerobic conditions. At each time point, the incubated samples were serially diluted and plated on NB agar plates (for MRSA), LB agar plates (for *P. aeruginosa*), TSB blood agar for *P. gingivalis* and *E. faecalis*,

and Columbia Blood agar using the Miles and Misra method to determine the CFU of each bacterial suspension.[56] The antimicrobial efficiency of the bioprinted scaffolds was evaluated based on the reduction in CFU over time. Untreated bacterial cultures and drug-free scaffolds were used as controls to assess the antimicrobial efficacy of the test scaffolds.

2.11 Biofilm inhibition assay

For the biofilm inhibition assay, samples were inoculated with diluted cultures following the same procedure used in the planktonic assays. The inoculated samples were incubated in a shaking incubator at 37 °C for 24 hours, with an anaerobic chamber utilized for *P. gingivalis*. After incubation, the samples were gently rinsed with phosphate-buffered saline (PBS) to remove non-adherent bacteria. Subsequently, the samples were sonicated for 15 minutes in 1 mL of LB, NB, or TSB broth to detach and resuspend the biofilms. The bacterial colony-forming units were then assessed by serially diluting the bacterial suspension and applying the Miles and Misra technique on LB, NB, and TSB blood agar plates.[56]

2.12 BDMDAC accelerated stability

Accelerated stability testing was conducted to evaluate the long-term stability of the scaffold over 3 months and 6 months using accelerated conditions.[57] The study was performed at an accelerated aging temperature of 40 °C, while the ambient real-time temperature (TRT) was set at 4 °C. A Q10 value of 2 was applied, and the accelerated aging factor (AAF) was calculated to be approximately 12.13. Based on this factor, 3 months of real-time stability was simulated in 7 days, and 6 months of real-time stability was simulated in 15 days. Scaffold samples were placed in a stability chamber at 40 °C, with evaluations conducted at the end of 7 and 15 days to assess key antimicrobial stability against MRSA, *P. aeruginosa*, *P. gingivalis*, *E. faecalis* and *S. mutans*. The antimicrobial efficacy of both freeze-dried and gel samples was assessed at 4 and 24 hours. For the stability study, only scaffolds containing the concentration of BDMDAC that achieved the minimum bactericidal concentration (MBC) at 4 and 24 hours in the planktonic assays were selected for evaluation. This method allowed for the efficient prediction of scaffold stability over extended periods, providing valuable insights within a shortened testing timeframe.

2.13 Cell viability

Human dental pulp stem cells (HDPSCs) used in this study were isolated from three donors' wisdom teeth (Leeds Dental and Skeletal Tissue Bank-DREC approval no. 251121/HA/366). Cells were cultured in alpha-modified minimum essential medium (alpha MEM) complete media, supplemented with 20% fetal bovine serum (FBS), 2 mM glutamine, 100 U penicillin/0.1 mg mL^{-1} streptomycin, and incubated at 37 °C, 5% CO_2. The media was changed every 5–7 days and sub-confluent cells (70–80%) were used in this study between passages 6 and 8.

Scaffold samples were divided into 4 test groups according to the concentration of BDMDAC incorporated in each sample, and one control group. Samples were first sterilised under UV light for 1 h. Indirect viability assay was carried out by incubating triplicate samples of each group of the scaffolds in 12 well plates with cell-free complete culture media, at three different time points (24 h, 72 h and 1 week). At each time of the time points, culture media was collected in sterile 1.5 ml Eppendorf tubes and frozen at −20 C. HDPSCs were seeded in a 96-well plate at a density of 1×10^4 cell per well and incubated with corresponding previously collected culture media for 48 hours. A negative control without cells and a positive control (untreated cells) were included in each experiment. After the incubation period, cell proliferation was assessed using an MTT Cell Proliferation Kit (Roche Applied Science, Penzberg, Germany). MTT labelling reagent was added to each well followed by 4 h incubation of the micro-plate in cell culture incubator at 37 °C and 5% CO_2. The formed formazan purple crystals were washed, solubilized in DMSO, solubilisation solution and incubated overnight to ensure complete solubilisation of the purple formazan crystals. The spectrophotometric absorbance of the samples was measured using a micro-plate reader, and the absorbance was read at 550 nm. Results were calculated from three independent experiments. The viability rates were calculated using the following formula:

$$\text{VR } \% = (\text{test OD} \times 100)/\text{positive control OD} \quad (6)$$

All cell proliferation assay experiments were carried out in 3 biological replicates from 3 different donors. Data were analysed using GraphPad Prism version 10. The mean values were compared between groups using two-way ANOVA and Tukey's multiple comparison test.

2.14 Statistical analysis

One-way analysis of variance (ANOVA) was used to compare whether the difference in antimicrobial efficiency and other measurements between each bioprinted sample was significantly different. A value of $p < 0.05$ was taken as being statistically significant.

3. Results and discussion

An antimicrobial biomaterial ink for 3D printing must exhibit effective antimicrobial activity, biocompatibility, and controlled therapeutic release. It should enable smooth extrusion, retain structural fidelity post printing and be non-cytotoxic to surrounding tissues. The ink must function as a reservoir for antimicrobial agents ensuring sustained and controlled release at therapeutically relevant concentrations.[58–60] This study focuses on optimizing these key parameters for the application of REPs.

3.1 Rheology

To elucidate the rheological behaviour of gelatin (GL) and gelatin-BDMDAC (GL-Q) biomaterial inks, a comprehensive

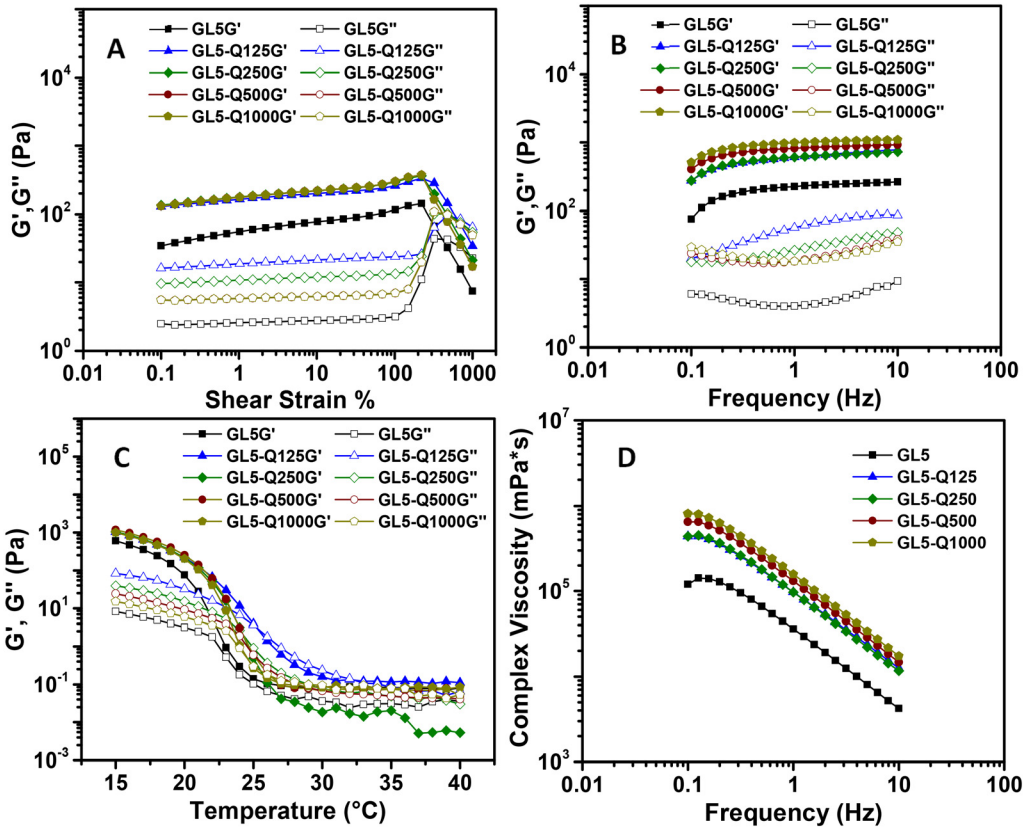

Fig. 1 Rheological analysis of gelatin/BDMDAC inks. (a) Amplitude sweep test. (b) Frequency sweep test. (c) Temperature dependence sweep. (d) Viscosity as a function of frequency. $N = 3$.

pre-printing analysis was conducted. Rheological measurements including strain amplitude response, frequency dependence in the linear viscoelastic regime (*i.e.*, small amplitude oscillatory shear limit), temperature profile, and complex viscosity was measured and the results are presented in Fig. 1 for the gelatin-BDMDAC inks (GL5-Q125, GL5-Q250, GL5-Q500, GL5-Q1000).

Amplitude sweep analysis (Fig. 1(A)) was performed at 21 °C over a strain range of 0.1–1000% to measure the viscoelastic properties. The graph depicts both the storage modulus (G') and loss modulus (G'') as functions of shear strain percentage. For all samples, at low shear strains, $G' > G''$, which indicates that the materials exhibit predominantly elastic behaviour within the linear viscoelastic region (LVR). As the strain increases, a critical strain point is reached where G' starts to decrease while G'' increases, signalling the onset of material yielding and the transition from a solid-like to a more viscous behaviour.

Frequency sweep test (Fig. 1(B)) were performed at 21 °C, with a fixed strain of 0.5%, further confirming the elastic dominance ($G' > G''$) across the 0.1–10 Hz range for both GL and GL-Q formulations. For the pure gelatin samples (GL5G′ and GL5G′), both G' and G'' show a slight frequency dependence, with moduli increasing gradually with frequency. This behaviour suggests a stable gel network with a balance between elasticity and viscosity. The gelatin-BDMDAC formulations (GL5-Q125G′, GL5-Q250G′, *etc.*), exhibited an increase both G' and G'', especially at higher frequencies, indicating BDMDAC enhances the material's resistance to deformation under rapid oscillatory shear (structural integrity).

Thermal stability was assessed *via* temperature sweeps (Fig. 1(C)) of the gelatin inks (GL5) and gelatin-BDMDAC formulation inks over a temperature range of 15 °C to 40 °C. For GL5, G' and G'' remain relatively high and stable at lower temperatures, indicating a well-structured, elastic gel network. However, as the temperature approaches around 26 °C, both moduli begin to decrease sharply, reflecting the thermal degradation of gelatin. This temperature marks the gel–sol transition, where the material shifts from a gel-like to a more fluid-like state.[61]

Complex viscosity profiles (Fig. 1(D)) indicate shear thinning behaviour where the complex viscosity decreases with increasing shear rate across all of the gelatin-BDMDAC (GL5-Q) samples.[61,62] This behaviour is typical of non-Newtonian fluids, indicating that the internal structure of the material becomes less resistant to flow under higher shear conditions (facilitating printing), likely due to the alignment or breakdown of molecular networks within the material.[61,62] Moreover, the complex viscosity of the samples shows a clear dependence on the concentration of GL5-Q. As the GL5-Q con-

centration increases, there is a corresponding increase in complex viscosity across all tested frequencies. This suggests that higher concentrations of GL5-Q lead to a more viscous solution. The increased viscosity can be attributed to the enhanced interaction between gelatin and BDMDAC molecules at higher concentrations, which likely results in a denser and more entangled network structure. This denser network increases the resistance to flow, hence the higher viscosity. At higher GL5-Q concentrations, the viscosity remains relatively high even at elevated frequencies, indicating a strong, cohesive network that resists deformation across a broad range of shear conditions.

3.2 Filament collapse test, diffusion rate and printability

The collapse area factor of gelatin-BDMDAC inks (GL-Q) is modulated by both BDMDAC concentration and distance value as shown in Fig. 2. The plot illustrates changes collapse area factor (%) changes with increasing distance value (mm) for five different GL5 material variants: GL5, GL5-Q125, GL5-Q250, GL5-500, and GL5-1000. Overall, most variants exhibit an increasing trend, where the collapse area factor rises as the distance increases, suggesting that larger distances (increment in deformation) lead to more significant collapses. The rate of increase, however, varies across the series. For instance, GL5-Q125 shows a gradual rise and even plateaus around the 4 to 5 mm mark, indicating material stability.

In contrast, GL5-500 and GL5-1000 exhibit sharper increases, implying these materials are more prone to larger collapses as the distance rises. Notably, the GL5-1000 variant has one of the highest collapse factors at 5 mm, suggesting it is more susceptible to structural failure. At 3 mm, all of the inks demonstrate a higher collapse factor compared to the control ink (GL5). This is an indication where the material becomes unstable and more prone to collapse as the concentration of BDMDAC is increased.

The plateau observed in some variants around 5 mm suggest that certain materials may reach an equilibrium point where further increases in distance no longer lead to significant collapses. The trend correlates with viscosity: higher BDMDAC concentrations yield increased viscosity, which enhances resistance to flow and deformation but compromises flexibility. Consequently, materials with higher concentrations of BDMDAC (GL5-500 and GL5-1000) more prone to fracture or collapse under stress, leading to larger collapse areas at higher distances.[45,47,48]

Lower BDMDAC concentrations, as in GL5-Q125 and GL5-Q250, result in reduced viscosity (Fig. 1(D)), yielding more pliable materials that are better able to absorb stress, thereby exhibiting a reduced collapsing factor. This can explain the more gradual rise in collapse area factor seen in these samples, as their lower viscosity allows them to distribute the applied forces more evenly.

The effect of BDMDAC concentration on filament diffusion and printability was assessed with eqn (2) and (3). Qualitatively, the most defined grids at the smallest grid spacing (2 × 2) was observed for GL5 and GL5-Q125, indicating superior print resolution. Quantitively, the diffusion rate (defined as the amount of material spread across a given grid area) served as an inverse indicator of print precision. A higher diffusion rate generally causes the material spreads more uncontrollably, which is detrimental to printing precision. For smaller grid spacings (*e.g.*, 1 × 1 mm^2), all GL5 variants show a high diffusion rate (~100%), indicating significant spread and reduced precision. With increased spacing, the diffusion decreases markedly for all formulations. However, GL5-Q1000 and GL5-Q500 retained a relatively higher diffusion rate compared to the other variants. This behaviour reflects the fact that higher viscosity materials resist flow and deformation more strongly but tend to diffuse more across smaller, confined spaces.[46]

Elevated diffusion rates correlated with reduced printing fidelity, as uncontrolled spreading leads to blurred or imprecise prints. Printability ratio, a metric of how accurately the material conforms to the intended grid, further illustrates this trend. As viscosity increases (from GL5-Q125 to GL5-Q1000), the printability ratio decreases at smaller grid spacings (1 × 1 mm^2 and 2 × 2 mm^2), reflecting the compromised print accuracy.[48] However at larger spacings (5 × 5 mm^2), differences between formulations diminish, indicating the impact of viscosity on print quality becomes less pronounced at broader feature scales (Fig. 3).[63]

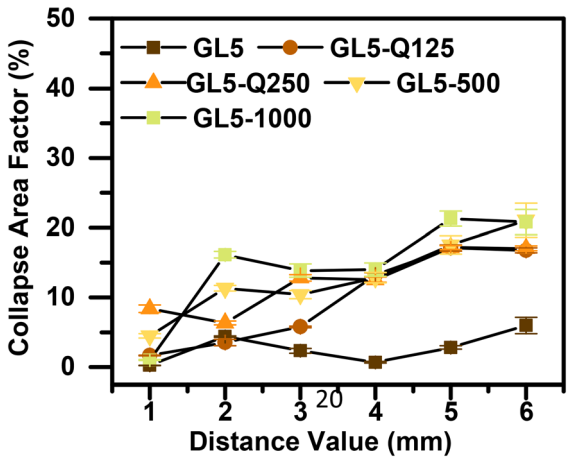

Fig. 2 Collapse area factor as a function of distance for all gelatin/BDMDAC inks.

3.3 Morphology (micro-CT)

X-ray micro-CT analysis was employed to examine the morphology and porosity of printed, freeze-dried, and re-hydrated gel samples, providing insights into their structural fidelity (Fig. 4). The printed gels maintained a high degree of shape accuracy throughout the process. Freeze-drying resulted in an average volumetric reduction of approximate 85% reduction in the overall volume of the printed gels. Notably, this volumetric shrinkage was accompanied by a nearly threefold increase in surface area due to the formation of additional porous structures. Upon re-hydration, the freeze-dried gels recovered approximately 80% of their original volume (Fig. 5). Despite

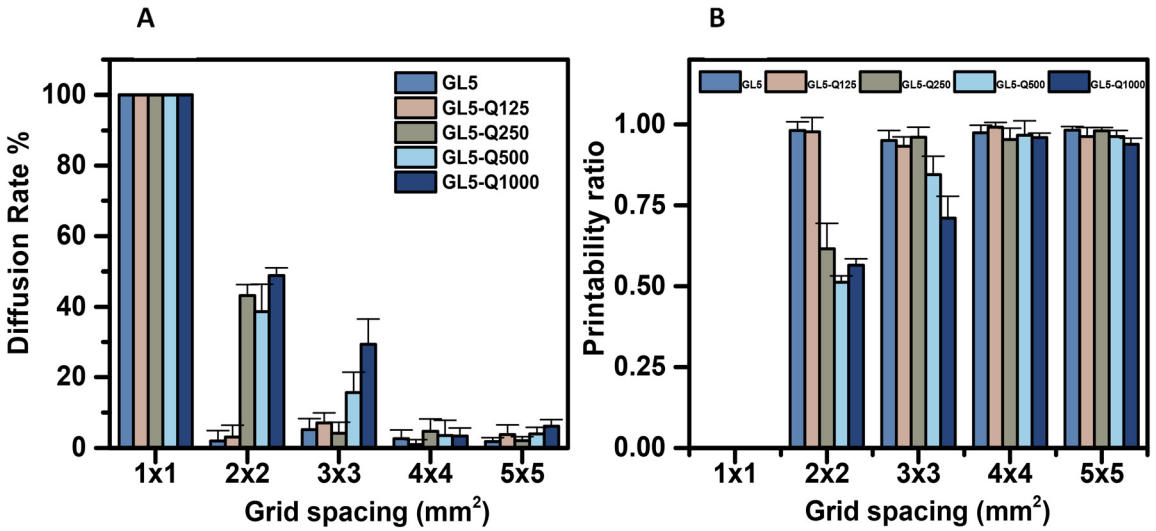

Fig. 3 Printability ratio (A) and diffusion rate percentage (B) of the GL5, GL5-Q125, GL5-Q250, GL5-Q500, GL5-1000 inks.

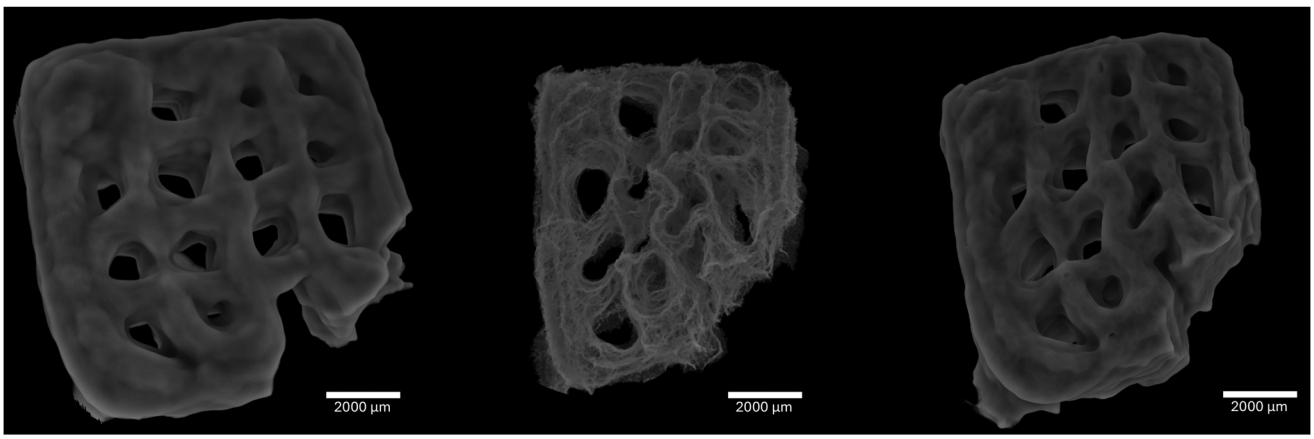

Fig. 4 X-ray CT scans depicting the structural changes of the gel at different stages of the process: recently printed (left), post freeze-drying (middle), and after re-hydration (right). To ensure consistent orientation across the scans, one corner of the sample was deliberately removed.

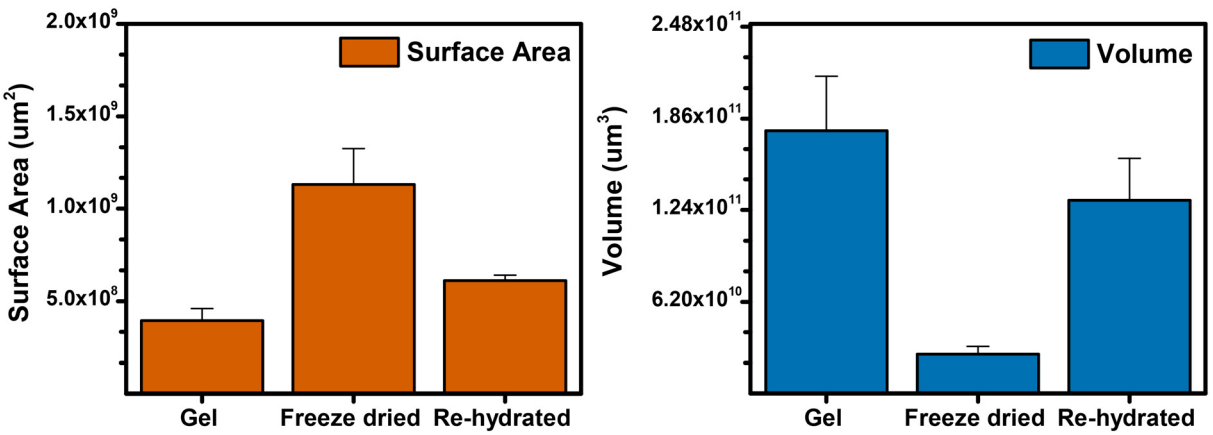

Fig. 5 Comparison of volume (left) and surface area (right) across different states—originally printed, freeze-dried, and re-hydrated. Measurements were obtained from X-ray CT analysis of whole-sample scans at a voxel resolution of 16.8 μm.

this volume recovery, the surface area remained elevated, measuring around 65% greater than that of the initially printed gel (Fig. 5). This suggests a persistent porous architecture post-rehydration.

Micro-CT analysis confirmed the internal porosity remained clearly detectable through even after the re-hydration process, highlighting the structural changes induced by freeze-drying and subsequent water absorption. High-resolution scans (4 μm voxel size) of a corner section of the printed sample revealed that freeze-drying significantly increased porosity (Fig. 6), reaching approximately 88%. This increase is consistent with the formation of a highly porous, interconnected network as water sublimation leaves behind void spaces. However, upon re-hydration, porosity was substantially reduced to around 31%, indicating a partial collapse or re-swelling of the porous network as water re-entered the structure.

The total number of pores decreased upon re-hydration, suggesting that smaller pores may have merged or collapsed as the gel reabsorbed water. Interestingly, changes in pore size distribution were not uniform across all samples. Some exhibited a shift toward smaller pores, likely due to the contraction of larger voids as the gel matrix rehydrated and partially regained its original conformation. In contrast, other samples maintained a similar pore size distribution, suggesting that factors such as localized variations in gel composition, cross-linking density, or drying kinetics could influence rehydration behavior.

This variability in pore structure following re-hydration may be attributed to sample handling and environmental conditions during preparation. Since hydration levels were not actively controlled after the initial re-hydration step, it is possible that partial drying occurred before μ-CT scanning, altering the observed pore structures. Additionally, differences in how individual samples responded to water absorption may reflect inherent heterogeneity in the gel network, with some regions more capable of retaining rehydrated water while others underwent irreversible structural changes due to the freeze-drying process.

In REPs, a thorough irrigation (typically by sodium hypochlorite) is essential for disinfecting the root canal by removing debris, biofilms, and microbial contaminants. Following rigorous irrigation and drying, commonly achieved with air or paper points, the BDMDAC-loaded scaffold can be inserted. This timing ensures minimal microbial contamination and enables the scaffold to provide sustained antimicrobial activity,

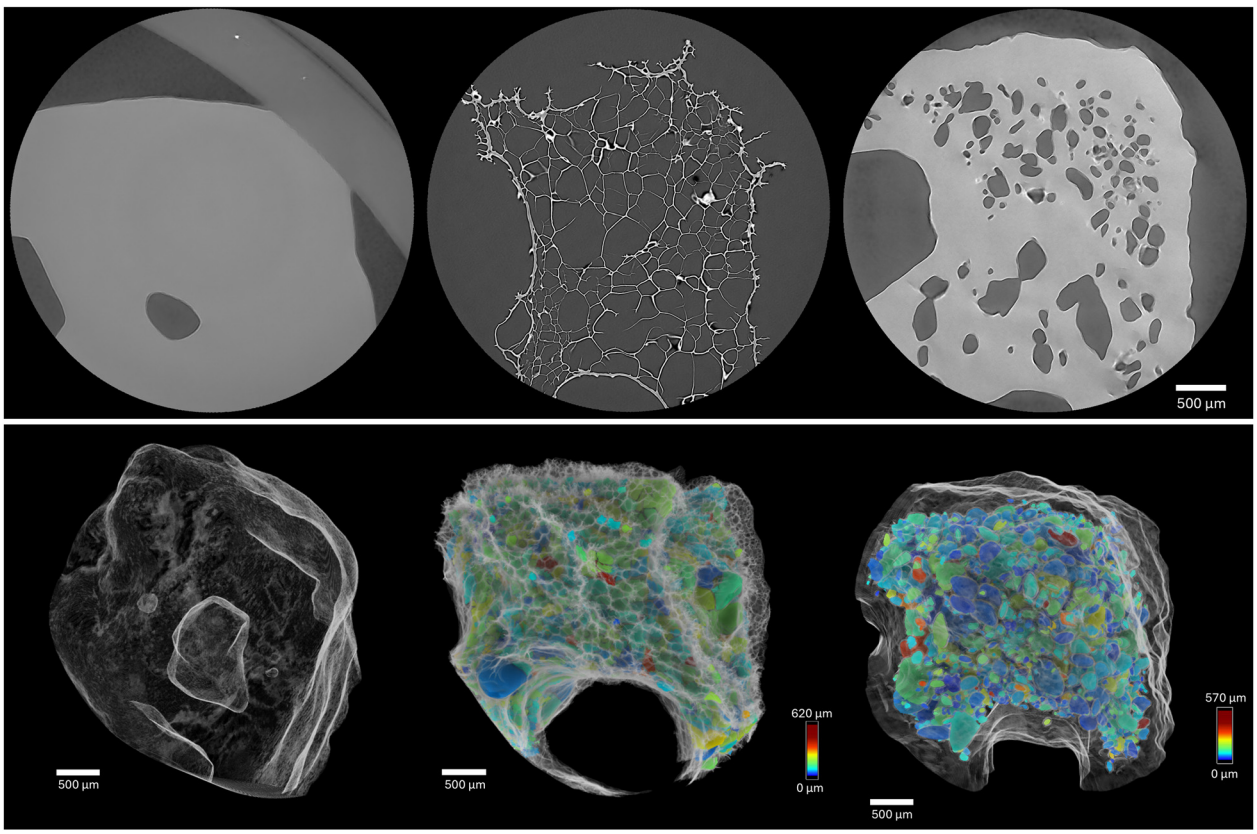

Fig. 6 Top: Representative cross-sectional slice images from high-resolution XCT scans (4 μm voxel size) of one corner of the same sample in three states— as-printed (left), freeze-dried (middle), and re-hydrated (right). Bottom: 3D renderings of the corresponding datasets. The as-printed gel exhibits minimal internal porosity (left). In the freeze-dried (middle) and re-hydrated (right) datasets, internal porosity has been segmented, with individual pores color-coded according to their size.

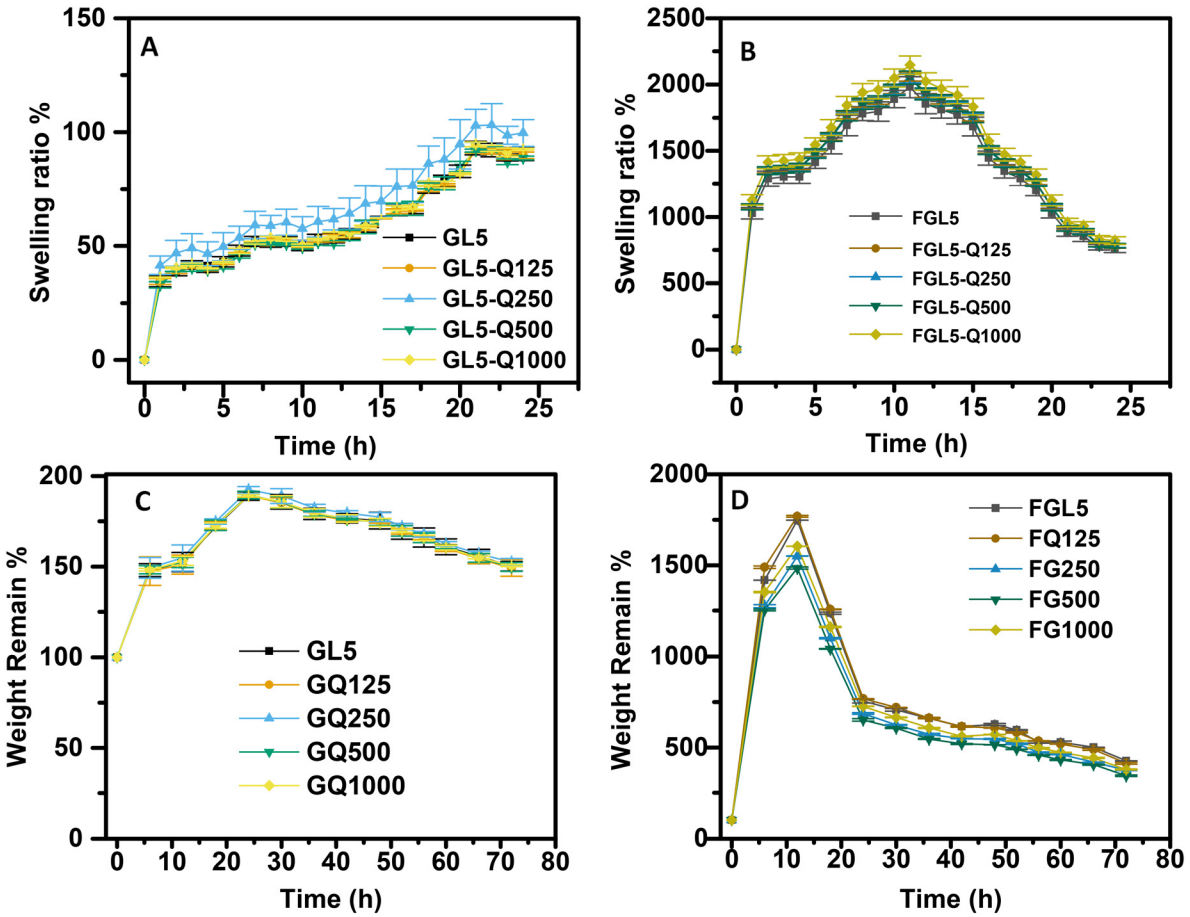

Fig. 7 (A) Swelling ratio of the gel scaffolds over a 24 hour period. (B) Swelling ratio of the freeze-dried scaffolds over a 24 hour period. (C) Degradation percentage of the gel scaffolds over a 72 hour period. (D) Degradation percentage of the freeze-dried scaffolds over a 72 hour period. $N = 3$.

complementing the initial disinfection and promoting tissue regeneration.

Compared to conventional injectable systems, 3D printed scaffolds offer several advantages, including patient-specific customization, controlled antimicrobial release, and optimized architecture for improved disinfection and tissue healing. In this study, grid-patterned scaffolds (10 × 10 × 2.5 mm, 20% infill) were employed to assess the mechanical, antimicrobial, and biocompatibility properties. Although these dimensions are not intended for clinical application, both the BDMDAC formulation and the 3D printing method are adaptable. Clinically relevant scaffolds would require a cylindrical or tapered geometry, with diameters of 0.5–1.5 mm and lengths of 8–15 mm, tailored to the root canal anatomy. Mechanical flexibility or compressibility would further support atraumatic placement.

To facilitate clinical translation, two delivery strategies are being explored: (1) a gel-based version extrudable *via* 3D printing for complex or curved canals, and (2) a freeze-dried, pre-shaped format derived from the gel, providing sterile, shelf-stable constructs that can be inserted using micro-forceps or conventional endodontic carriers. Furthermore, advances in imaging technologies such as CBCT and micro-CT further support the creation of patient-specific scaffolds, enhancing precision and therapeutic outcomes in REPs (Fig. 7).

3.2 Swelling and degradation

The swelling behaviour of both gel-based and freeze-dried scaffolds demonstrates no significant relationship with increasing BDMDAC concentration. Across all tested formulations, (Table 1) scaffolds with varying BDMDAC concentrations (Table 1) exhibit similar swelling profiles. Although swelling ratios increase over time, the values for different BDMDAC concentrations remain within standard deviations of each other, indicating no statistically significant difference from gelatin-BDMDAC scaffolds to their pure gelatin controls. In freeze-dried samples, swelling peaks at around 15 hours and then slightly declines. These findings suggest that the incorporation of BDMDAC does not markedly influence the swelling capacity of gelatin-based scaffolds in either hydrated or freeze-dried form.

The degradation behaviour, measured as the percentage of weight remaining over time, also shows no significant effect of BDMDAC concentration. Both the gel-based and freeze-dried

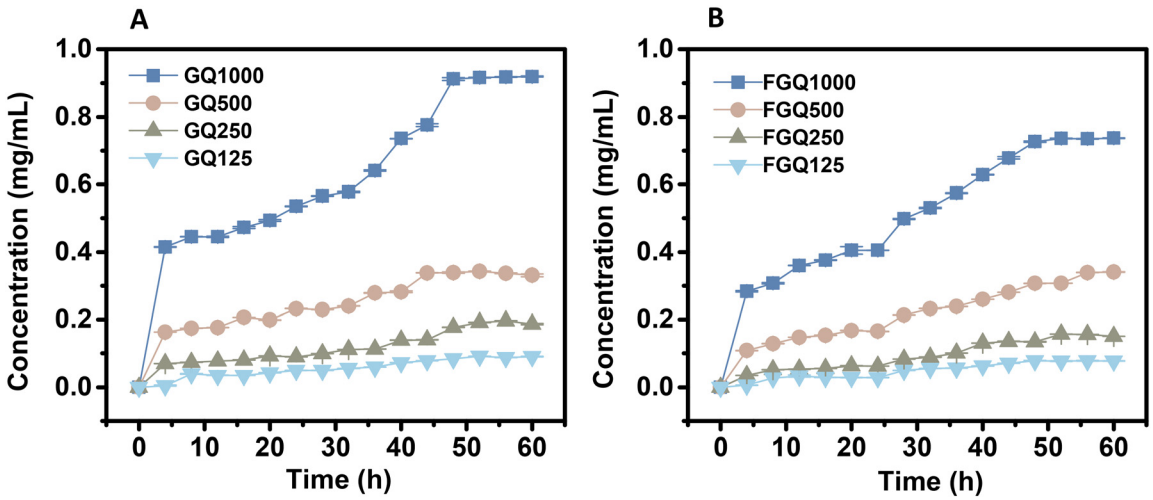

Fig. 8 Gelatin/BDMDAC release over a 60-hour period measured by high performance liquid chromatography for gel scaffolds (A) and freeze-dried scaffolds (B). N = 3.

scaffolds, exhibit comparable degradation profiles. The gel samples show minimal differences in degradation across BDMDAC concentrations. The degradation profiles exhibit a maximum weight peaking around 30–40 hours before gradually decreasing. Similarly, freeze-dried scaffolds show a sharp initial weight loss in the first 10 hours, followed by stabilization and a gradual decline in weight remaining, with little variation between BDMDAC-modified and unmodified scaffolds. This may be due to due to the initial leaching of loosely bound material, after which weight loss stabilises and carries on at a slower rate. Across all BDMDAC concentrations, there is no difference in the degradation pattern, indicating that BDMDAC modification does not compromise the long term long-term structural stability of the scaffolds (Fig. 8).

3.4 BDMDAC release

The release profiles of BDMDAC from gel and freeze-dried scaffolds, as measured by HPLC, demonstrate a controlled, sustained release correlating to the initial concentration. Scaffolds with higher concentrations of BDMDAC (1000 μg mL^{-1}) exhibit a more pronounced and rapid release over time, reaching nearly 1 mg mL^{-1} by the 60 hour mark. In contrast, the lower concentrations (500 μg mL^{-1}, 250 μg mL^{-1}, and 125 μg mL^{-1}) display more gradual release patterns, characterised with distinct plateaus. The release rate is slow during the initial phase, followed by a noticeable acceleration at approximately 40 h, reaching a plateau shortly after. Although, both the gel and freeze-dried scaffolds display broadly similar release profiles, there are potential variations in their release kinetics. Specifically, freeze-dried scaffolds might may display a slightly faster initial release, likely due to a more porous structure or altered diffusion dynamics.[64] The overall trends in both scaffold types indicate a reliable, prolonged release of BDMDAC, with the highest concentration samples consistently outperforming the lower ones in terms of total release. Overall, both scaffold formats allow for reliable and prolonged delivery of BDMDAC, with higher initial concentrations consistently generating greater cumulative release (Fig. 9).

3.5 Antimicrobial planktonic assay

The antimicrobial efficacy of the gel and freeze-dried scaffolds was investigated at 4 and 24 hours against *MRSA*, *Pseudomonas aeruginosa* and three dental pathogens: *Porphyromonas gingivalis*, *Enterococcus faecalis* and *Streptococcus mutans*. Against *MRSA*, the lower concentration gel scaffold (GL5-Q7.8) took 24 hours to achieve complete kill, the higher concentration scaffold (GL5-Q15) achieved complete kill in only 4 h. Following freeze-drying, only the higher concentrated scaffold (FGL5-Q15) achieved complete kill at 4 and 24 hours. Against *P. aeruginosa*, both GL5-Q250 and FGL5-Q250 displayed similar efficacy achieving a 2-log reduction at 4 hours and a 5-log reduction at 24 hours. For *P. gingivalis*, both GL5-Q31 and FGL5-Q31 showed comparable performance, with a 1-log reduction at both time points. In the case of *E. faecalis*, a much higher QAC concentration, GL5-Q125 and FGL5-Q125 were required to achieve complete kill at 4 and 24 hours. GL5-Q62 and FGL5-Q62 performed similarly at 4 hours with a 2-log reduction, but at 24 hours, the bacteria regrew and only a 1-log reduction was observed. Lastly, for *S. mutans*, both GL5-Q125 and FGL5-Q125 achieved the minimum bactericidal concentration (MBC). Notably, while the GL5-Q62 and FGL5-Q62 showed similar effects at 4 hours, the freeze-dried sample showed an additional 1-log reduction at 24 hours.

In this study, both gel-based and freeze-dried samples displayed comparable antimicrobial performance overall. However, notable pathogen specific differences were observed. For MRSA, the gel samples outperformed the freeze-dried ones. At the 4-hour mark, GL5-Q7.8 achieved complete bacterial eradication, whereas FGL5-Q7.8 resulted in a 2-log reduction. By 24 hours, GL5-Q7.8 showed a 1-log reduction,

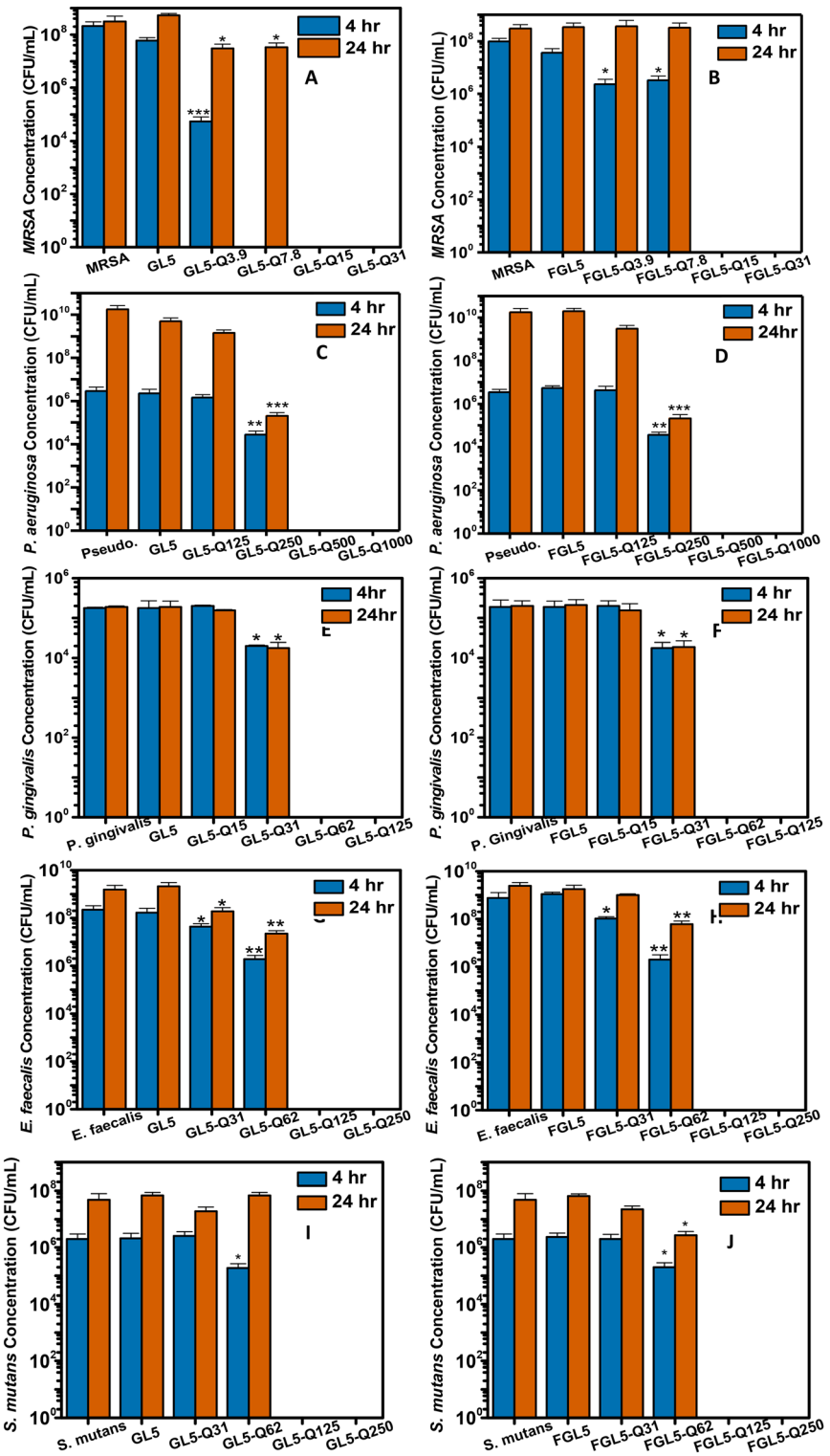

Fig. 9 Planktonic inhibition assay of BDMDAC-incorporated gel and freeze-dried scaffolds at 4 hour and 24 hour time points against four bacterial strains: (A, C, E, G and I) gel scaffolds and (B, D, F, H and J) freeze-dried scaffolds against MRSA, *Pseudomonas aeruginosa*, *Porphyromonas gingivalis*, *Enterococcus faecalis*, and *Streptococcus mutans*. $N = 3$ *$p < 0.001$,**$p < 0.001$, ***$p < 0.001$.

while FGL5-Q7.8 exhibited no further reduction. For *P. aeruginosa*, *P. gingivalis*, and *E. faecalis*, both GL5-Qx and FGL5-Qx performed equally at both time points. However, for *S. mutans*, FGL5-Q62 demonstrated a 1-log reduction compared to GL5-Q62 at 24 hours, though both samples behaved similarly at the 4-hour mark.

The precise antimicrobial mechanism by of QACs is not fully understood, but the prevailing theory suggests a "contact killing" process. QACs like BDMDAC feature a long, hydrophobic chain which enable them to penetrate and disrupt the bacterial cell membrane. Upon contact, QACs attach to the cell wall, disrupt and integrate in to the lipid bilayer, compromising the membrane's integrity. This leads to leakage of the cellular contents, membrane disintegration, and eventually bacterial death (Fig. 10).[26]

Gram-positive bacteria are characterized by a porous peptidoglycan-rich, loosely packed outer layer making them susceptible to QAC penetration. The polymer chains more easily penetrate this layer, reaching the cytoplasmic membrane, causing cellular damage. Conversely, Gram-negative bacteria possess an additional outer membrane composed of a lipid bilayer. This extra barrier shields the inner membrane, rendering Gram-negative bacteria more resistant to the effects of QACs.[26]

3.7 Antimicrobial biofilm inhibition assay

The biofilm inhibition capacity of different concentrations of BDMDAC was evaluated for several bacteria species at 24 hours in both gel-based (GL5) and freeze-dried scaffolds (FGL5). For MRSA, lower concentrations of BDMDAC ($\leq$ 7.8 μg mL^{-1}) did not result in significant biofilm inhibition. Complete eradication was observed at highest concentrations, GL5-Q15 and GL5-Q31, for both GL5 and FGL5 forms, indicating that these concentrations are highly effective in inhibiting MRSA biofilms after 24 hours.

For *P. aeruginosa*, significant biofilm inhibition was observed at BDMDAC concentrations of 500 μg mL^{-1} and above. Specifically, GL5-Q500 achieved a 5-log reduction and complete kill for GL5-Q1000 and FGL5-Q1000. Across all lower concentrations, the gel-based scaffolds (GL5) demonstrated greater anti-biofilm efficacy compared to their freeze-dried counterparts (FGL5), with the exception of the highest concentration, where both formats performed equally. The reduced efficacy in the FGL5 samples could be cue to the higher porosity of these samples which potentially promotes bacterial colonisation and biofilm formation. The increased porosity leading to increased bacterial adhesion can potentially lead to flow obstruction when bacterial load gets high. This accumulation of bacteria can promote the formation of protective biofilm environments, which limit antimicrobial penetration, reduce diffusion efficiency, and ultimately lower bacterial eradication rates.[65] Notably, there was no significant inhibition at GL5-Q125 and FGL5-Q125.

The antimicrobial effect of BDMDAC on *P. gingivalis* was less pronounced compared with the other bacterial species. For *E. faecalis*, both the gel-based and freeze-dried forms demonstrated moderate biofilm inhibition, with GL5-Q62 and FGL5-Q62 showing significant reductions in biofilm formation. Higher BDMDAC concentrations were more effective, with GL5-Q125, FGL5-Q125, GL5-Q250 and FGL5-Q250 achieving complete biofilm inhibition. No significant inhibition was observed at concentrations up to 62 μg mL^{-1} for both gel and freeze-dried forms. Complete kill was observed for higher concentration samples, GL5-Q125, FGL5-Q125, GL5-Q250 and FGL5-Q250. For *S. mutans*, a 1 log reductions were observed at GL5-Q62, while no significant inhibition was observed for the freeze-dried form. For higher concentrations both gel and freeze-dried forms demonstrated complete kill.

QACs are broad-spectrum, nonspecific antibacterial agents that primarily disrupt bacterial cell membranes and exhibit anti-biofilm activity.[66] For example, Gaspar *et al.*, suggest that dequalinium chloride, a type of QAC, diffuses into the cells, and exerts lytic effect leading to biofilm destruction.[67] Similarly, Joseph *et al.*, reported that water soluble positively charged ammonium cationic pillararenes inhibit biofilm assembly without damaging cell membranes.[68] Furthermore, Jung and colleagues have demonstrated that the use of water soluble amphiphilic quaternary ammonium chitosans not only kill individual cells but also bind to preformed biofilms, thereby, increasing the local concentration of antimicrobial agents.[69]

In the root canal environment, *E. faecalis* exhibits a remarkable ability to withstand harsh conditions and form biofilms on the inner surfaces of tooth canals, making it exceptionally difficult to eliminate.[38] These characteristics contribute to its high prevalence in secondary and persistent endodontic infections.[35] *P. gingivalis* is a Gram-negative, black-pigmented anaerobe is implicated in periodontal disease, abscesses and endodontic infections[70–72] *S. mutans* is one of the main species associated with dental carries and is often found in primary and secondary/persistent endodontic infections.[73,74] The ability of these 3D printed scaffolds to target all of these infections is promising for their clinical viability for the treatment of REPs (Fig. 11).

3.6 Accelerated stability studies

The present study evaluated the antimicrobial efficacy of GL5-Qx and FGL5-Qx, determining the MBC for each of the 4 bacteria species over a three- and six-month period. Both gel-based and freeze-dried scaffolds demonstrated significant antimicrobial activity against all tested bacteria, including MRSA, *E. coli*, *S. mutans*, and *P. aeruginosa*.

The freeze-dried scaffold FGL5-Qx consistently demonstrated strong antimicrobial activity throughout the study. At the 3 month mark, FGL5-Qx achieved complete antimicrobial efficacy at the 4 and 24 h time points. The only exception was *E. faecalis* at 4 hours, which exhibited a 4-log reduction in bacterial count. At 6 months, a slight reduction in antimicrobial efficacy was observed at the 4 hour time point, with a 3-log reduction against both *E. faecalis* and *S. mutans*. Despite this decline, the scaffold maintained its full efficacy at 24 hours against all bacterial species, indicating that while there is a minor loss of rapid antimicrobial activity over time, the scaffold retains its long-term effectiveness. This finding suggests that the freeze-dried scaffold may gradually lose some of its immediate antimicrobial potency, but it continues to offer robust and sustained effects.

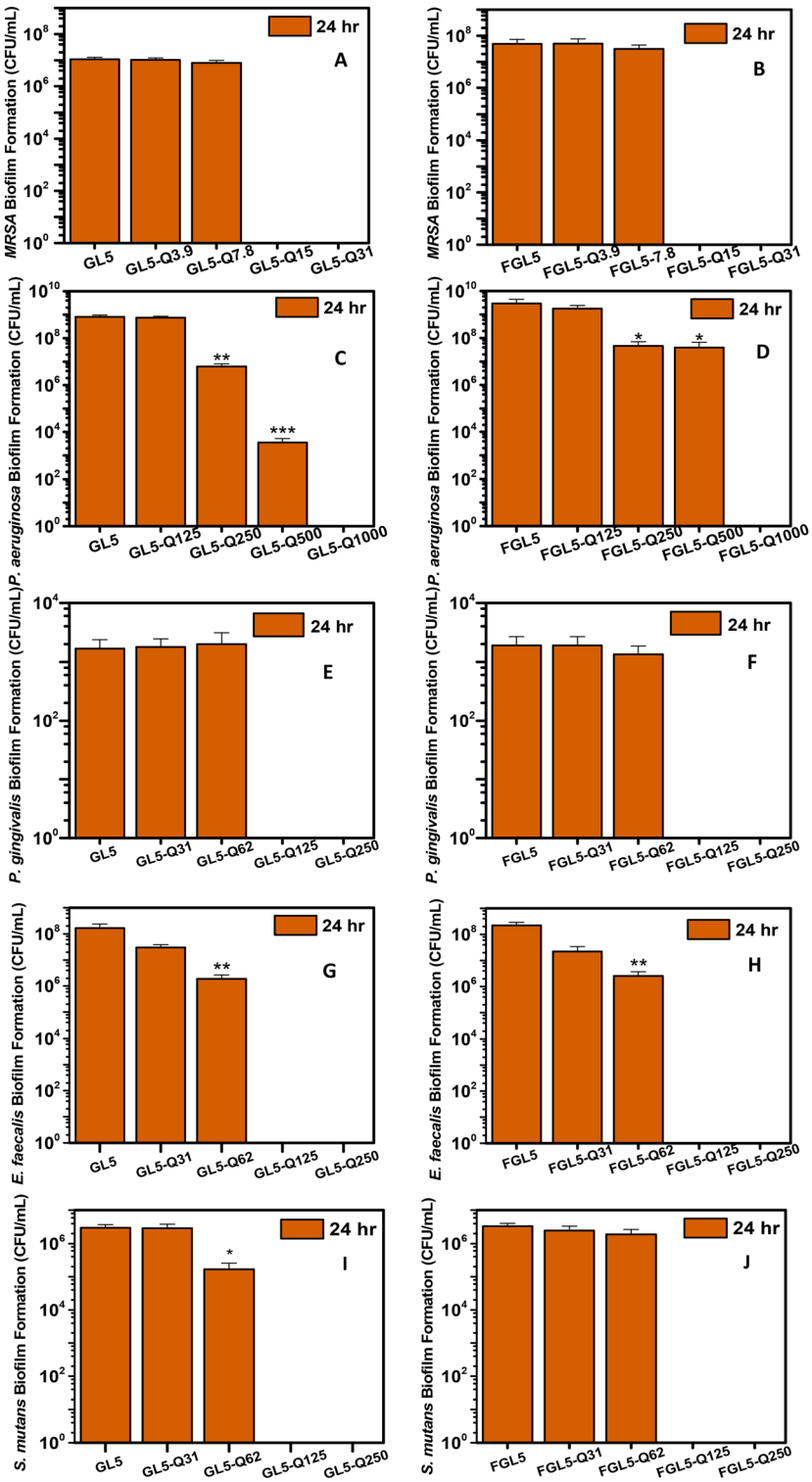

Fig. 10 Biofilm inhibition assay of BDMDAC-incorporated gel and freeze-dried scaffolds at a 24-hour time point against four bacterial strains: (A, C, E, G and I) gel scaffolds and (B, D, F, H and J) freeze-dried scaffolds against MRSA, *Pseudomonas aeruginosa*, *Porphyromonas gingivalis*, *Enterococcus faecalis*, and *Streptococcus mutans*. $N = 3$ *$p < 0.001$,**$p < 0.001$, ***$p < 0.001$.

The gel samples, GL5-Qx, demonstrated significant antimicrobial activity; albeit with a reduced efficacy compared with the freeze-dried formulation, FGL5-Qx. At 3-month mark, GL5-Qx showed reduced efficacy at the 4 hour time point, with a 2-log reduction against *E. faecalis*, a 3-log reduction against *S. mutans*, and a 4-log reduction against *P. aeruginosa*, in contrast to the more potent activity seen with FGL5-Qx. Additionally, at the 3 month, 24 hour point, GL5-Qx displayed

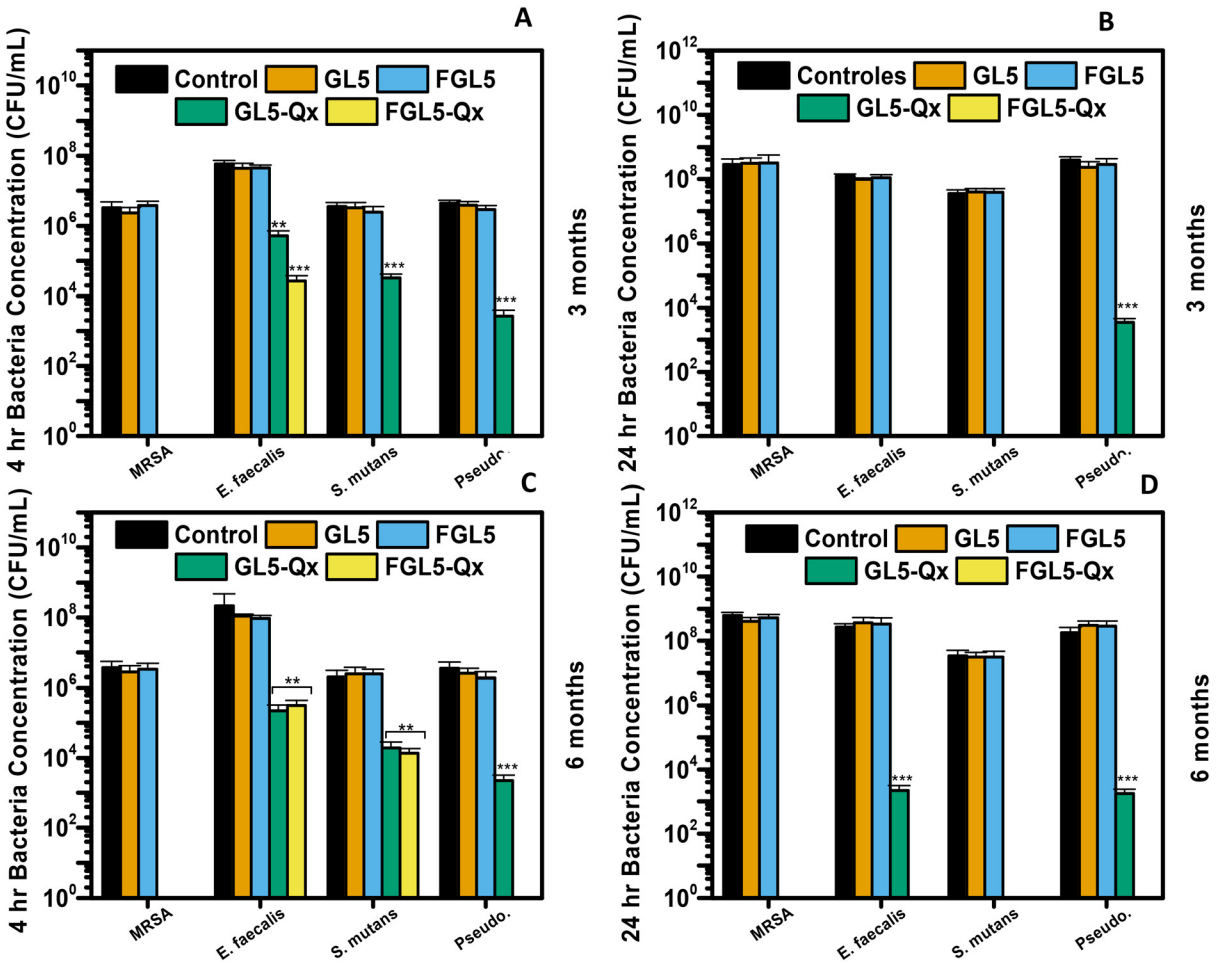

Fig. 11 Stability assessment of BDMDAC-incorporated gel and freeze-dried scaffolds *via* planktonic inhibition assays at 3-month and 6-month intervals, conducted at 4-hour and 24 hour time points for MRSA, *Pseudomonas aeruginosa*, *Enterococcus faecalis*, and *Streptococcus mutans*, using minimum bactericidal concentrations: 15.6 μg mL^{-1} for MRSA, 500 μg mL^{-1} for *Pseudomonas aeruginosa*, 62.5 μg mL^{-1} for *Enterococcus faecalis*, and 125 μg mL^{-1} for *Streptococcus mutans*. (A) 4 hour inhibition at 3 months. (B) 24 hour inhibition at 3 months. (C) 4-hour inhibition at 6 months. (D) 24 hour inhibition at 6 months. $^{**}p < 0.001$, $^{***}p < 0.001$.

reduced antimicrobial efficacy against *P. aeruginosa*, achieving only a 4-log reduction compared to the complete efficacy of FGL5-Qx. This diminished activity could be attributed to alterations in the physical properties of the scaffold due to dehydration, which may affect its stability and the bacterial susceptibility profile during storage. Despite these reductions, GL5-Qx still exhibited strong antimicrobial activity against the tested bacterial species, indicating its potential as a viable antimicrobial agent, though less robust than its freeze-dried counterpart. This suggests that formulation stability plays a critical role in maintaining antimicrobial efficacy over time (Fig. 10 and 11).

3.9 Cell viability

The impact of the 3D printed freeze-dried scaffolds on cell viability was accessed using human primary dental pulp stem cells from three donor patients to evaluate their potential use in REPs. Freeze-dried scaffolds with concentrations of 0, 125, 250, 500, and 1000 μg mL^{-1} were evaluated. Lower concentrations that were effective against only MRSA were excluded as these scaffolds need to be effective against a broad range of pathogens with higher MBCs. Cell viability was assessed using a standard MTT assay (GL5, GL5-Q125, GL5-Q250, GL5-Q500, GL5-Q1000) at three time points (24 hours, 72 hours, and 1 week) in accordance with ISO-10993-5 standards. For the scaffolds to be considered non-cytotoxic, cells must maintain >70% viability.

The results demonstrated a concentration-dependent cytotoxic effect of BDMDAC-loaded scaffolds (Fig. 12). At 24 hours, all sample types demonstrated a decrease in cell viability compared to the control samples, with higher BDMDAC concentrations leading to a further decrease in viable cells. However, cell viability in most groups increased at the 72 hour time point. Notably, the GL5-Q125 and the GL-Q250 samples had over 70% viable cells after 1 week in culture indicating no cytotoxicity and would be potential formulations to take forward for further biological evaluation. The findings of this study highlight the importance of carefully considering the concen-

tration of BDMDAC incorporated into scaffolds to balance antimicrobial activity with biocompatibility. While higher BDMDAC concentrations may provide enhanced antimicrobial protection, they may also increase the cytotoxicity. This study focuses on cell viability for an indication of cytotoxicity. The focus of future work is to undertake a comprehensive evaluation of HDPSC stemness, proliferation, and differentiation to validate the full therapeutic potential of these scaffolds.

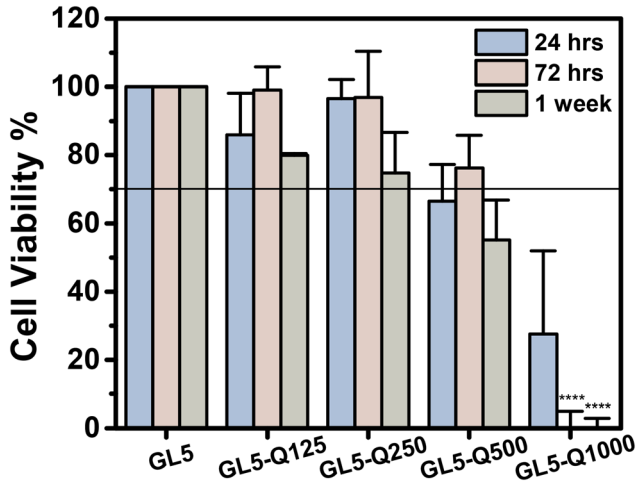

Fig. 12 Indirect effect of QCA on the Percentage of HDPSC proliferation after 24 h, 72 h and 1 week of exposure showing the percentage of HDPSC proliferation at the different time points *p = 0.0378, **p = 0.0025, ****p < 0.0001.

4. Conclusion

This study reports on the development of biocompatible 3D printed hydrogel scaffolds for the effective disinfection of a root canal space for regenerative endodontic procedures. The physicochemical properties of 3D printed scaffolds were comprehensively studied in terms of the rheological behaviour, stability, swelling, degradation and printability. The release of BDMDAC from the scaffolds demonstrated release over a 60 hr time period. Antimicrobial efficacy was assessed against 5 pathogens (MRSA, *P. aeruginosa*, *P. gingivalis*, *E. faecalis* and *S. mutans*) in the planktonic and biofilms adhered states, revealing a concentration dependent activity, with *P. aeruginosa* being the most difficult to kill. The freeze-dried scaffold FGL5-Qx showed strong antimicrobial activity, achieving high efficacy against all tested bacteria within 4 and 24 hours at 3 months. The GL5-Q125 (125 μg mL^{-1}) and GL5-Q250 (250 μg mL^{-1}) samples exhibited broad spectrum activity against widest range of pathogens tested and maintained over 70% cell viability of human dental pulp stem cells (HDPSC) at 24 h and 72 h. These BDMDAC-loaded gelatin scaffolds show exceptional antimicrobial efficacy, particularly against *E. faecalis*, with no cytotoxicity toward HDPSC. Overall these results highlight a strong clinical potential for these scaffolds to be used for root canal disinfection in regenerative endodontic applications.

Author contributions

Mateo Dallos Ortega: writing – original draft, validation, methodology, investigation, formal analysis, data curation. Jenny Aveyard: writing – review & editing, visualization, validation, supervision, methodology, funding acquisition, formal analysis, conceptualization. Raghda M Abdelgawad: writing – review & editing, methodology, investigation Reem El-Gendy: writing – review & editing, methodology, data curation, supervision. Alexander Ciupa: writing – review & editing, methodology, investigation, data curation. David Whetnall: writing – review & editing, methodology, investigation, data curation. Julia Behnsen: writing – review & editing, methodology, investigation, data curation. Robert J. Poole: writing – review & editing, validation, supervision. Raechelle A. D'Sa: writing – review & editing, visualization, validation, supervision, resources, project administration, funding acquisition, conceptualization.

Data availability

The data that support the findings are available on request from the first author (Mateo Dallos Ortega m.dallos@liverpool.ac.uk) and corresponding author (Raechelle D'Sa r.dsa@liverpool.ac.uk).

Conflicts of interest

There are no conflicts to declare.

Acknowledgements

This research was supported by the Engineering and Physical Sciences Research Council (EP/W016389/1). The Zeiss Xradia Versa 620 was provided under EPSRC strategic equipment grant number EP/V007610/1. M. D. O. thanks the Colombian Government Scholarship MinTec 885. The graphical abstract was created using Biorender.

References

1 J. O. Andreasen, *et al.*, A long-term study of 370 autotransplanted premolars. Part II. Tooth survival and pulp healing subsequent to transplantation, *Eur. J. Orthod.*, 1990, **12**(1), 14–24.
2 B. N. Lee, *et al.*, A review of the regenerative endodontic treatment procedure, *Restor. Dent. Endod.*, 2015, **40**(3), 179–187.
3 H. F. Duncan, *et al.*, Treatment of pulpal and apical disease: The European Society of Endodontology (ESE) S3-level clinical practice guideline, *Int. Endod. J.*, 2023, **56**(S3), 238–295.

4 Procedures., A.A.o.E.C.c.f.r. [cited 2025 24/04], Available from: https://www.aae.org/uploadedfiles/publications_and_research/research/currentregenerativeendodonticconsiderations.pdf.
5 M. Nakashima and K. Iohara, Regeneration of dental pulp by stem cells, *Adv. Dent. Res.*, 2011, **23**(3), 313–319.
6 V. Rosa, *et al.*, Dental pulp tissue engineering in full-length human root canals, *J. Dent. Res.*, 2013, **92**(11), 970–975.
7 J. A. Mateo Dallos Ortega, A. Ciupa, R. J. Poole, D. Whetnall and R. A. D'Sa, *Printable gelatin/nisin antimicrobial hydrogel ink for 3D bioprinting and tissue engineering applications*, 2024.
8 M. T. P. Albuquerque, J. Nagata and M. C. Bottino, Antimicrobial Efficacy of Triple Antibiotic-eluting Polymer Nanofibers against Multispecies Biofilm, *J. Endod.*, 2017, **43**(9s), S51–S56.
9 A. A. Ayoub, *et al.*, Electrospun Azithromycin-Laden Gelatin Methacryloyl Fibers for Endodontic Infection Control, *Int. J. Mol. Sci.*, 2022, **23**(22), 13761.
10 A. Karczewski, *et al.*, Clindamycin-modified Triple Antibiotic Nanofibers: A Stain-free Antimicrobial Intracanal Drug Delivery System, *J. Endod.*, 2018, **44**(1), 155–162.
11 J. Palasuk, *et al.*, Bimix antimicrobial scaffolds for regenerative endodontics, *J. Endod.*, 2014, **40**(11), 1879–1884.
12 C. Liu, *et al.*, Long-term exposure to pro-inflammatory cytokines inhibits the osteogenic/dentinogenic differentiation of stem cells from the apical papilla, *Int. Endod. J.*, 2016, **49**(10), 950–959.
13 P. Verma, *et al.*, Effect of Residual Bacteria on the Outcome of Pulp Regeneration In Vivo, *J. Dent. Res.*, 2017, **96**(1), 100–106.
14 L. Vishwanat, *et al.*, Effect of Bacterial Biofilm on the Osteogenic Differentiation of Stem Cells of Apical Papilla, *J. Endod.*, 2017, **43**(6), 916–922.
15 A. S. Kharchi, N. Tagiyeva-Milne and S. Kanagasingam, Regenerative Endodontic Procedures, Disinfectants and Outcomes: A Systematic Review, *Prim. Dent. J.*, 2020, **9**(4), 65–84.
16 R. Sellami, *et al.*, Regenerative endodontic procedures in immature permanent teeth with pulp necrosis: the impact of microbiology on clinical and radiographic outcome, *Front. Dent. Med.*, 2023, **4**, 1–12.
17 W. Almutairi, *et al.*, Regenerative Endodontics: A Systematic Analysis of the Failed Cases, *J. Endod.*, 2019, **45**(5), 567–577.
18 T. M. Botero, *et al.*, Clinical Evidence for Regenerative Endodontic Procedures: Immediate versus Delayed Induction?, *J. Endod.*, 2017, **43**(9s), S75–S81.
19 M. C. M. Conde, *et al.*, A scoping review of root canal revascularization: relevant aspects for clinical success and tissue formation, *Int. Endod. J.*, 2017, **50**(9), 860–874.
20 K. M. Galler, *et al.*, Influence of root canal disinfectants on growth factor release from dentin, *J. Endod.*, 2015, **41**(3), 363–368.
21 A. R. Diogenes, *et al.*, Translational science in disinfection for regenerative endodontics, *J. Endod.*, 2014, **40**(4 Suppl), S52–S57.
22 S. M. F. Lima, *et al.*, Antimicrobial and immunomodulatory activity of host defense peptides, clavanins and LL-37, in vitro: An endodontic perspective, *Peptides*, 2017, **95**, 16–24.
23 S. S. Namazi, *et al.*, Multifunctional and biodegradable methacrylated gelatin/Aloe vera nanofibers for endodontic disinfection and immunomodulation, *Biomater. Adv.*, 2023, **150**, 213427.
24 M. C. Jennings, K. P. C. Minbiole and W. M. Wuest, Quaternary Ammonium Compounds: An Antimicrobial Mainstay and Platform for Innovation to Address Bacterial Resistance, *ACS Infect. Dis.*, 2015, **1**(7), 288–303.
25 Y. Li, *et al.*, Applications of quaternary ammonium compounds in the prevention and treatment of oral diseases: State-of-the-art and future directions, *J. Dent.*, 2023, **137**, 104678.
26 P. Makvandi, *et al.*, Antibacterial quaternary ammonium compounds in dental materials: A systematic review, *Dent. Mater.*, 2018, **34**(6), 851–867.
27 S. Imazato, *et al.*, Antibacterial resin monomers based on quaternary ammonium and their benefits in restorative dentistry, *Jpn. Dent. Sci. Rev.*, 2012, **48**(2), 115–125.
28 N. Izutani, *et al.*, Antibacterial effects of MDPB against anaerobes associated with endodontic infections, *Int. Endod. J.*, 2010, **43**(8), 637–645.
29 N. Hirose, *et al.*, Development of a Cavity Disinfectant Containing Antibacterial Monomer MDPB, *J. Dent. Res.*, 2016, **95**(13), 1487–1493.
30 S. Kumar Tiwari, *et al.*, The inhibitory effect of quaternary ammonium salt on bacteria in root canal, *Sci. Rep.*, 2019, **9**(1), 12463.
31 J. S. Ribeiro, *et al.*, Photocrosslinkable methacrylated gelatin hydrogel as a cell-friendly injectable delivery system for chlorhexidine in regenerative endodontics, *Dent. Mater.*, 2022, **38**(9), 1507–1517.
32 J. S. Ribeiro, *et al.*, Engineering of Injectable Antibiotic-laden Fibrous Microparticles Gelatin Methacryloyl Hydrogel for Endodontic Infection Ablation, *Int. J. Mol. Sci.*, 2022, **23**(2), 1–15.
33 J. F. Siqueira Jr and I. N. Rôças, Diversity of endodontic microbiota revisited, *J. Dent. Res.*, 2009, **88**(11), 969–981.
34 I. N. Rôças and J. F. Siqueira Jr, Identification of bacteria enduring endodontic treatment procedures by a combined reverse transcriptase-polymerase chain reaction and reverse-capture checkerboard approach, *J. Endod.*, 2010, **36**(1), 45–52.
35 J. F. Siqueira Jr and I. N. Rôças, Distinctive features of the microbiota associated with different forms of apical periodontitis, *J. Oral Microbiol.*, 2009, **1**, DOI: 10.3402/jom.v1i0.2009.
36 Y. L. Ng, *et al.*, Outcome of primary root canal treatment: systematic review of the literature - part 1. Effects of study characteristics on probability of success, *Int. Endod. J.*, 2007, **40**(12), 921–939.
37 E. K. Sirén, *et al.*, In vitro antibacterial effect of calcium hydroxide combined with chlorhexidine or iodine potass-

ium iodide on Enterococcus faecalis, *Eur. J. Oral Sci.*, 2004, **112**(4), 326–331.
38 C. H. Stuart, *et al.*, Enterococcus faecalis: its role in root canal treatment failure and current concepts in retreatment, *J. Endod.*, 2006, **32**(2), 93–98.
39 G. Dahlén, *et al.*, Identification and antimicrobial susceptibility of enterococci isolated from the root canal, *Oral Microbiol. Immunol.*, 2000, **15**(5), 309–312.
40 R. S. Eddy, *et al.*, An in vitro evaluation of the antibacterial efficacy of chlorine dioxide on E. faecalis in bovine incisors, *J. Endod.*, 2005, **31**(9), 672–675.
41 I. Portenier, *et al.*, The susceptibility of starved, stationary phase, and growing cells of Enterococcus faecalis to endodontic medicaments, *J. Endod.*, 2005, **31**(5), 380–386.
42 K. Nakajo, *et al.*, Resistance to acidic and alkaline environments in the endodontic pathogen Enterococcus faecalis, *Oral Microbiol. Immunol.*, 2006, **21**(5), 283–288.
43 L. S. Mokeem, *et al.*, Benzyldimethyldodecyl Ammonium Chloride Doped Dental Adhesive: Impact on Core's Properties, Biosafety, and Antibacterial/Bonding Performance after Aging, *J. Funct. Biomater.*, 2022, **13**(4), 190.
44 C.-C. Kuo, *et al.*, An integrated manufacturing strategy to fabricate delivery system using gelatin/alginate hybrid hydrogels: 3D printing and freeze-drying, *Food Hydrocolloids*, 2021, **111**, 106262.
45 A. Habib and B. Khoda, Development of clay based novel hybrid bio-ink for 3D bio-printing process, *J. Manuf. Process.*, 2019, **38**, 76–87.
46 D. Therriault, S. R. White and J. A. Lewis, Rheological Behavior of Fugitive Organic Inks for Direct-Write Assembly, *Appl. Rheol.*, 2007, **17**(1), 10112–1–10112–8.
47 G. Gillispie, *et al.*, Assessment methodologies for extrusion-based bioink printability, *Biofabrication*, 2020, **12**(2), 022003.
48 A. Ribeiro, *et al.*, Assessing bioink shape fidelity to aid material development in 3D bioprinting, *Biofabrication*, 2017, **10**(1), 014102.
49 J. Schindelin, *et al.*, Fiji: an open-source platform for biological-image analysis, *Nat. Methods*, 2012, **9**(7), 676–682.
50 R. Domander, A. A. Felder and M. Doube, BoneJ2 - refactoring established research software, *Wellcome Open Res.*, 2021, **6**, 37.
51 D. Legland, I. Arganda-Carreras and P. Andrey, MorphoLibJ: integrated library and plugins for mathematical morphology with ImageJ, *Bioinformatics*, 2016, **32**(22), 3532–3534.
52 A. Limaye, Drishti: a volume exploration and presentation tool. Proc. SPIE 8506, Developments in X-Ray Tomography VIII, 85060X (October 17, 2012), 2012.
53 S. M. Bittner, *et al.*, Swelling Behaviors of 3D Printed Hydrogel and Hydrogel-Microcarrier Composite Scaffolds, *Tissue Eng., Part A*, 2021, **27**(11–12), 665–678.
54 D. Bociaga, *et al.*, Sodium Alginate/Gelatine Hydrogels for Direct Bioprinting-The Effect of Composition Selection and Applied Solvents on the Bioink Properties, *Materials*, 2019, **12**(17), 2669.
55 D. R. Lonsway, Preparation of Routine Media and Reagents Used in Antimicrobial Susceptibility Testing, in *Clinical Microbiology Procedures Handbook*, Wiley, 2023, DOI: 10.1002/9781683670438.cmph0082.
56 A. A. Miles, S. S. Misra and J. O. Irwin, The estimation of the bactericidal power of the blood, *J. Hyg.*, 1938, **38(6)**, 732–749.
57 M. Huelsmeyer, *et al.*, A universal tool for stability predictions of biotherapeutics, vaccines and in vitro diagnostic products, *Sci. Rep.*, 2023, **13**(1), 10077.
58 N. Ashammakhi, *et al.*, Bioinks and bioprinting technologies to make heterogeneous and biomimetic tissue constructs, *Mater. Today Bio*, 2019, **1**, 100008.
59 A. R. Akkineni, *et al.*, Controlled and Local Delivery of Antibiotics by 3D Core/Shell Printed Hydrogel Scaffolds to Treat Soft Tissue Infections, *Pharmaceutics*, 2021, **13**, 2151.
60 H. Wang, *et al.*, An Overview of Extracellular Matrix-Based Bioinks for 3D Bioprinting, *Front. bioeng. biotechnol.*, 2022, **10**, 905438.
61 M. Bercea, Rheology as a Tool for Fine-Tuning the Properties of Printable Bioinspired Gels, *Molecules*, 2023, **28**(6), 2766.
62 D. A. Rau, M. J. Bortner and C. B. Williams, A rheology roadmap for evaluating the printability of material extrusion inks, *Addit. Manuf.*, 2023, **75**, 103745.
63 M. Rueda, *et al.*, Rheology and applications of highly filled polymers: A review of current understanding, *Prog. Polym. Sci.*, 2016, **66**, 22–53.
64 W. S. W. Shalaby, G. E. Peck and K. Park, Release of dextromethorphan hydrobromide from freeze-dried enzyme-degradable hydrogels, *J. Controlled Release*, 1991, **16**(3), 355–363.
65 K. Z. Coyte, *et al.*, Microbial competition in porous environments can select against rapid biofilm growth, *Proc. Natl. Acad. Sci. U. S. A.*, 2017, **114**(2), E161–E170.
66 E. A. Saverina, *et al.*, From Antibacterial to Antibiofilm Targeting: An Emerging Paradigm Shift in the Development of Quaternary Ammonium Compounds (QACs), *ACS Infect. Dis.*, 2023, **9**(3), 394–422.
67 C. Gaspar, *et al.*, Dequalinium Chloride Effectively Disrupts Bacterial Vaginosis (BV) *Gardnerella* spp, Biofilms, *Pathogens*, 2021, **10**(3), 261.
68 R. Joseph, *et al.*, Cationic Pillararenes Potently Inhibit Biofilm Formation without Affecting Bacterial Growth and Viability, *J. Am. Chem. Soc.*, 2016, **138**(3), 754–757.
69 J. Jung, J. Wen and Y. Sun, Amphiphilic quaternary ammonium chitosans self-assemble onto bacterial and fungal biofilms and kill adherent microorganisms, *Colloids Surf., B*, 2019, **174**, 1–8.
70 M. Haapasalo, *et al.*, Black-pigmented Bacteroides spp. in human apical periodontitis, *Infect. Immun.*, 1986, **53**(1), 149–153.

71 A. D. Haffajee and S. S. Socransky, Microbial etiological agents of destructive periodontal diseases, *Periodontology 2000*, 1994, **5**, 78–111.
72 A. J. van Winkelhoff, A. W. Carlee and J. de Graaff, Bacteroides endodontalis and other black-pigmented Bacteroides species in odontogenic abscesses, *Infect. Immun.*, 1985, **49**(3), 494–497.
73 E. T. Pinheiro, *et al.*, Microorganisms from canals of root-filled teeth with periapical lesions, *Int. Endod. J.*, 2003, **36**(1), 1–11.
74 I. N. Rôças and J. F. Siqueira Jr, Frequency and levels of candidate endodontic pathogens in acute apical abscesses as compared to asymptomatic apical periodontitis, *PLoS One*, 2018, **13**(1), e0190469.